RSC Advances

PAPER

View Article Online
View Journal | View Issue

Cite this: *RSC Adv.*, 2020, **10**, 9347

The green exfoliation of graphite waste and its suitability for biosensor applications

Tarek H. Taha,*[a] Mohamed S. Elnouby,*[b] M. A. Abu-Saied[c] and Saad Alamri[de]

Received 18th November 2019
Accepted 5th January 2020

DOI: 10.1039/c9ra09602g

rsc.li/rsc-advances

This work is concerned with the bio-exfoliation of graphite using a soil bacterium. The isolated bacterium showed a detectable ability to oxidize and change its physical appearance and chemical structure. Multiple characterization procedures were used to study the physical and chemical changes. Raman and FTIR spectroscopy proved that the isolate G3 partially exfoliated the graphite into multi-layer sp^2 graphitic layers. Scanning electron microscopy (SEM) proved that there was a change in morphology between untreated graphite waste and that manipulated by bacteria. Cyclic voltammetry results proved that the green exfoliated graphite (GEG) was suitable for use in biosensor applications and showed a noticeable ability to detect methanol, even at lower concentrations. These findings are considered as promising for the biological manipulation of graphite waste for environmental purposes. In addition, it is proved that the bacterial transformation of graphite into other GEG structures occurs without needing the chemically hazardous methods that are currently applied.

Introduction

Recently, nanomaterial-based analytical methods have gained continuous attention for use in different applications, such as: biological research, medicinal and pharmaceutical analysis, food safety and environmental monitoring. Nanomaterials are considered as potential analytical probes, owing to their high surface-to-volume ratio, exceptional physicochemical properties, high adsorption and reactive capacity and other beneficial properties not present in bulk materials.[1]

Various nanomaterials have been employed to serve various functions in the design of biosensors. A biosensor is a compact analytical device which relies on the immobilization of biomolecules on a transducer surface.[2] Among the various types of biosensors available, electrochemical biosensors offer numerous advantages over conventional methods due to their simplicity, high sensitivity, and rapidity.

Graphene is considered to have the highest surface-to-volume ratio with an optical transparency of 97% that results from its existence as a single layer consisting of one-atom thickness.[3] Its electrical and thermal conductivities are currently reported to be superior to most conductive elements such as silver, copper and gold.[4,5] These powerful, thermal, mechanical, and electrical properties suggest that it is possible to use graphene in various applications such as batteries, hydrogen storage, bioanalytics, photocatalysis, drug carriers, and sensors.[6–11] The two predominant methods that include chemical vapor deposition (CVD) and exfoliation are mainly used for the preparation of graphene. However, there are several drawbacks to using the CVD method because it is expensive and difficult to scale up for use industrially.[12,13] The exfoliation method is composed of two steps: the first one is the oxidation of graphite into graphene oxide followed by its reduction into reduced graphene oxide or graphene as the second step.[14,15] However, the second step involves the use of hazardous substances such as hydrazine which adds undesired nitrogen groups onto the surface and shows elevated energy demands.[16,17]

There is a wide distribution of ethanol in many applications including alcoholic beverages and liquid cosmetics, and it is not harmful in small quantities. However, methanol can be converted into strongly toxic metabolites which can cause damage to the nervous system and finally lead to death.[18] In some countries, commercial fraud is used to blend methanol with alcoholic beverages instead of ethanol to reduce the production costs. The serious problem comes from the fact that both alcohols have the same physical properties and cannot easily be distinguished. Therefore, finding a reliable method to detect small amounts of methanol in ethanol is essential.[19]

[a]*Environmental Biotechnology Department, Genetic Engineering and Biotechnology Research Institute (GEBRI), City of Scientific Research and Technological Applications (SRTA-City), New Borg El-Arab City, 21934, Alexandria, Egypt. E-mail: t.h.taha@gmail.com*

[b]*Composite and Nanostructured Materials Research Department, Advanced Technology and New Materials Research Institute, City of Scientific Research and Technological Applications (SRTA-City), New Borg El-Arab City, 21934, Alexandria, Egypt. E-mail: m_nano2050@yahoo.com*

[c]*Polymer Materials Research Department, Advanced Technology and New Materials Research Institute, City of Scientific Research and Technological Applications (SRTA-City), New Borg El-Arab City, 21934, Alexandria, Egypt*

[d]*Department of Biology, College of Science, King Khalid University, P. O. Box 9004, Abha, Saudi Arabia*

[e]*Research Center for Advanced Materials Science (RCAMS), King Khalid University, P. O. Box 9004, Abha 61413, Saudi Arabia*

The aim of the current work is concerned with maximizing the benefits of graphite waste and reducing its undesired environmental impacts. It depends on the isolation of a bacterial isolate that can manipulate the graphite powder waste and convert it, using green chemistry, into other precious and eco-friendly forms such as the GEG structure. The work was extended to characterize the carbonic structure obtained by instrumental analysis using Raman, Fourier transform infrared (FTIR) and SEM techniques. The benefits of the structure obtained were investigated by testing its ability to be used as biosensor for the detection of environmental hazardous materials such as methanol especially at very low concentrations.

Experimental work

Graphite waste

The graphite waste (G0) was obtained as unused powder that originated by cutting a big graphite bar into small electrodes prepared for electrochemical applications at City of Scientific Research and Technological Applications.

Sample preparation

Soil samples were collected from different locations at the New Borg El-Arab City. Each sample was serially diluted from 10^{-1} to 10^{-7} using sterile normal saline.

Isolation of graphite manipulating bacteria

The isolation of graphite manipulating bacteria was dependent on the ability of bacterial isolates to grow on Luria–Bertani agar plates (LB) supplemented with graphite powder. In the beginning, LB agar medium was prepared and supplemented with 0.25 g L^{-1} graphite powder. The prepared LB-graphite bottle was autoclaved at 115 °C and 6.9 kPa for 20 min. After sterilization, the agar medium was poured into sterile Petri plates and transferred into 4 °C for solidification. Soil dilutions were spread over the plates with a sterile glass spreader using 50 μL of each dilution. The plates were incubated at 30 °C for three days. The formed bacterial colonies were picked up and purified on LB agar plates and considered as presumptive graphite manipulating bacteria.

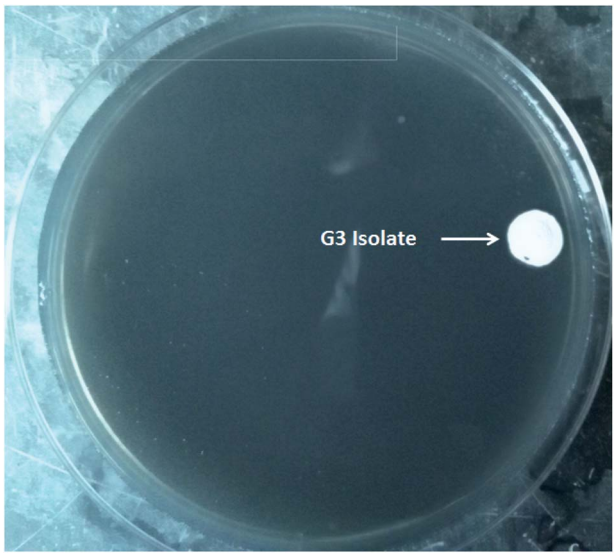

Fig. 1 The ability of the G3 isolate to grow on a graphite-containing agar plate.

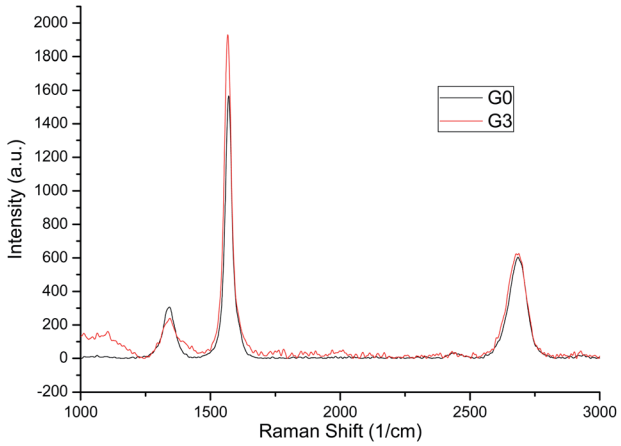

Fig. 2 Raman spectra of samples G0 and GEG (G3).

Liquid broth manipulation process

The purified isolated graphite manipulating bacteria were re-cultivated in a graphite containing broth medium for the examination of their real ability to bio-convert graphite into other carbon structures. The process was dependent on the inoculation of 1 mL of microbes grown overnight in 10 mL of sterile minimal broth containing (g L^{-1}): NaCl, 0.5; K_2HPO_4, 0.3; KH_2PO_4, 0.4; yeast extract, 0.1; distilled H_2O, 1000 mL, and with addition of 0.25 g L^{-1} of graphite. The flasks were incubated at 30 °C and 150 rpm for 72 h.

Lysis of bacterial cells

After incubation, the bacterial cells were lysed and washed out leaving the transformed carbon structure in a pure form for subsequent characterization. The lysis procedure started with

Table 1 A summary of the Raman parameters

Band		G0	GEG
D	Peak	1342	1343.5
	I_D	306.9264	239.5548
	FWHM	51.561	68.374
G	Peak	1570	1567
	I_G	1566.78	1929.771
	FWHM	30.649	32.476
	I_D/I_G	0.195896	0.124136
2D	Peak	2685	2688
	I_{2D}	602.861	624.8059
	I_{2D}/I_G	0.384777	0.32377
	FWHM	77.695	84.986
	R^2	0.936	0.9368

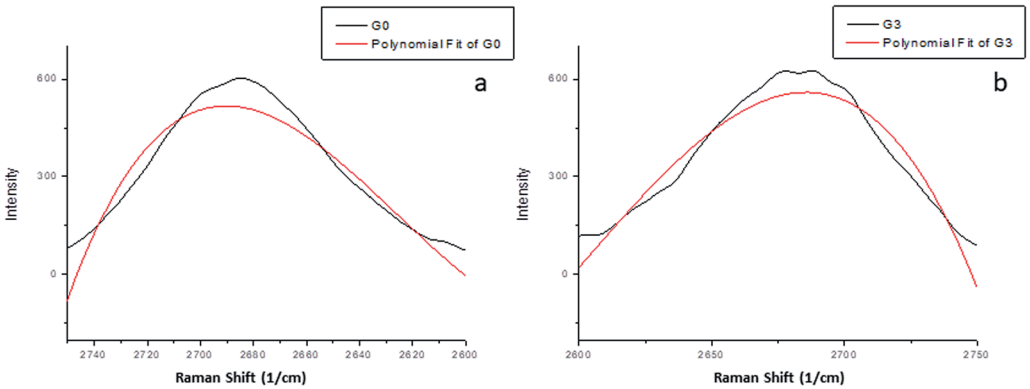

Fig. 3 Raman 2D bands of (a) graphite (G0) and (b) GEG (G3); both plots show the measured data profile fit.

centrifugation of the culture containing bacterial cells at 6000 rpm for 5 min, followed by removal of the supernatant. The carbon-bacterial pellets formed were dispersed in 2 mL of 10% sodium dodecyl sulfate solution (SDS) for 30 min at 50 °C, followed by centrifugation at 6000 rpm for 5 min. The supernatant was discarded and the pellets were washed twice with 1 mL of absolute ethanol and once with 1 mL of distilled water with centrifugation at 6000 rpm after each washing step. The carbonic pellets were finally air dried and were submitted for the instrumental characterization.

Microbial identification

DNA extraction. DNA of the isolate G3 was extracted using the Amshag DNA extraction kit according to the instruction manual (SRTA City, Egypt).

Amplification and sequencing of the 16S rRNA gene. The PCR amplification of the 16S rRNA gene of the isolate G3 was achieved using universal primers. The PCR components were composed of 12.5 μL of master mix (Takara Bio, Japan), 1 μL of forward primer (27F) 5′-AGAGTTTGATCMTGGCTCAG-3′, 1 μL of reverse primer (1492R) 5′-TACGGYACCTTGTTACGACT-3′, and 1 μL of extracted DNA. The amplified gene was checked by migration through 1.5% agarose gel in 1× TBE buffer followed by UV visualization and photography using a UV trans-illuminator and gel documentation system (SynGene, Germany). The specific band was excised from the agarose gel, purified, sequenced, and submitted to GenBank to be compared with the other genes deposited in its database. The sequence obtained was then deposited in GenBank under a specific accession number.

Characterizations

Structural characterizations. The morphological structures of the graphite and GEG powders were performed using SEM (JSM-6360LA, Jeol, Japan). The chemical structures of the graphite and GEG powders were investigated by Raman scattering spectrometer (Senterra, Bruker, Germany) and Fourier transform infrared (FTIR) spectroscopy (FTIR-8400S, Shimadzu, Japan).

Electrochemical characterization. The graphite powder before and after exfoliation was used to fabricate an electrochemical working electrode as follows: 2.5 mg of both powders were dispersed separately in a solution containing 50 μL of Nafion (10 wt%) in 450 μL of isopropyl alcohol. Each suspension was sonicated in an ultrasonic bath for about 30 min. A portion (10 μL) of the homogeneous prepared ink was drop coated on a previously polished glassy carbon electrode.

The electrochemical experiments were conducted on a potentiostat (Autolab 87070, Metrohm) in a three electrode configuration system. All electrochemical experiments were carried out in a cell containing 100 mL of phosphate buffered

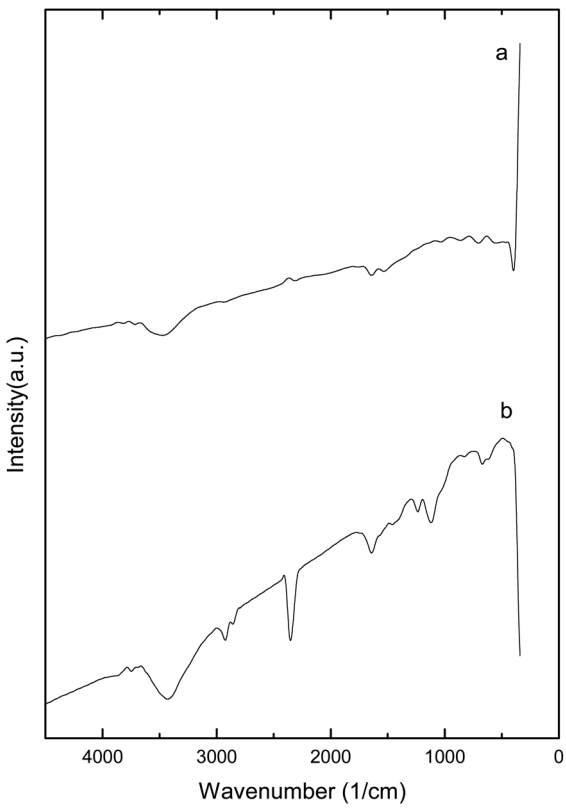

Fig. 4 FTIR spectra of (a) graphite powder and (b) GEG powder.

saline solution (PBS, pH 7.0) or 100 mL of ethanol. Each electrolyte was amended with different doses of methanol (0–1.0 mL/100 mL). A graphite rod was used as the auxiliary electrode, an Ag/AgCl wire as the reference electrode, together with the previously prepared working electrode.

Results and discussion

Isolation of graphite manipulating bacteria

After the cultivation and incubation of serially diluted soil on the graphite containing plate, the grown bacterial isolates were collected up and purified. As shown in Fig. 1, only one isolate was able to grow and formed a single white big colony. This bacterial isolate was considered as the presumptive graphite manipulating isolate and was transferred to graphite containing broth to confirm its ability to manipulate the graphite.

Raman spectroscopy

Raman spectroscopy is considered to be a fast and non-destructive method, which provides a direct understanding of the electron–phonon interactions, which indicate a high sensitivity to electronic and crystallographic structures.[20] Fig. 2 compares the Raman spectra of samples G0 and GEG measured at 532 nm excitation. The three most intense peaks were observed at ~1340 cm^{-1} (D band), ~1570 cm^{-1} (G band) and ~2670 cm^{-1} (2D band).

The D band is recognized as the disorder, or defect band, whereas, the G band is the results of an in-plane vibrational mode of the sp^2 hybridized carbon atoms that comprise graphene sheets.[20] Raman spectra could be used to characterize the level of disorder in carbon nanostructures using the peak ratio of I_D/I_G. Herein, this ratio decreased from 0.195896 to 0.124136 which may be due to the increasing defect density.

However, the 2D band is at almost double the frequency of the D band and originates from the second order Raman scattering process. This band is used to determine the graphene layer thickness, and the degree of defects could be confirmed by using the ratio I_{2D}/I_G. In the present study this ratio was 0.384777 and 0.32377 for the graphite and GEG samples, respectively. Al-Sherbini *et al.*, prepared graphene sheets with a high number of defects and a large number of graphene layers were exfoliated from graphite with an I_{2D}/I_G of 0.46.[20]

Herein, these peaks hardly shifted. The full width at half maximum (FWHM) together with the intensity of the peaks could express more about the structure. Table 1 summarizes the positions, intensity and FWHM for the main three peaks for both samples. Sample GEG has a much broader and upshifted 2D band with respect to the G0 sample, which indicated that GEG has multilayered graphene formed form graphite (G0).[21] Moreover, the 2D band of graphene was more uniform compared to that of the graphite sample as shown in Fig. 3.[22]

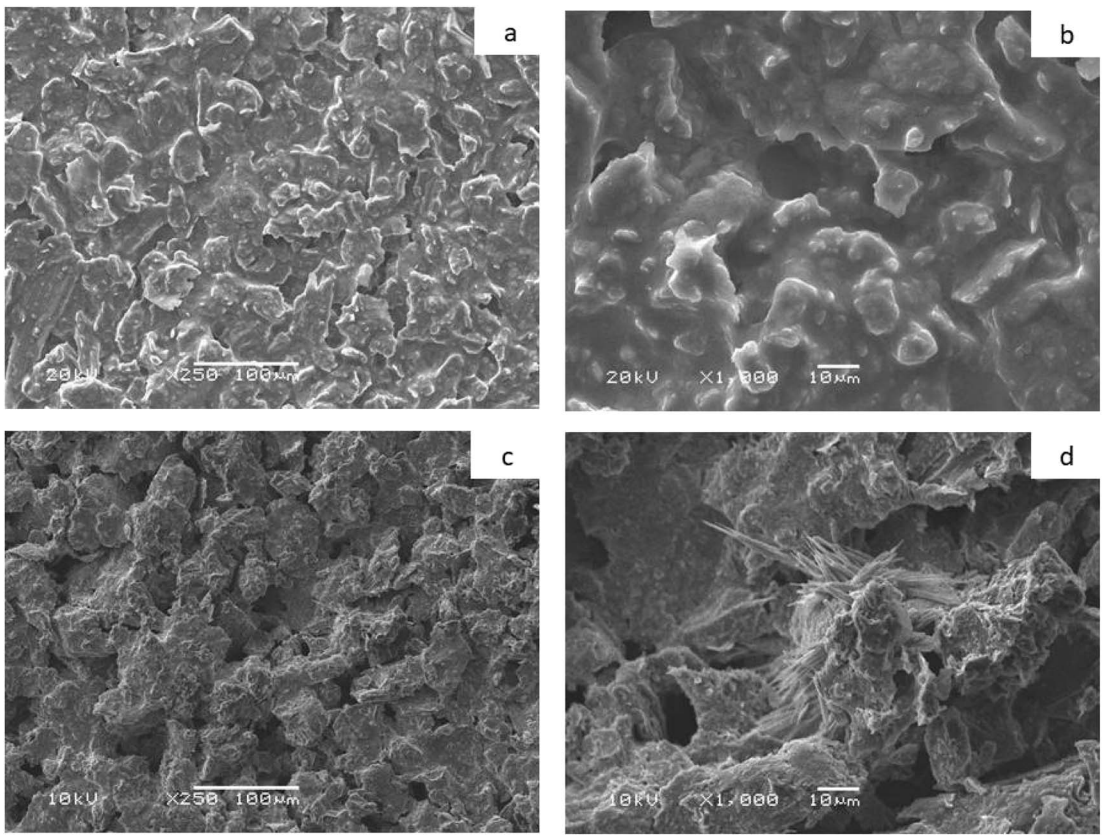

Fig. 5 SEM micrographs: (a and b) low and high magnification images of graphite powder, and (c and d) low and high magnification images of GEG.

Roscher *et al.*, reported that, the R^2 value of graphene was higher than that of graphite.[23]

FTIR analysis

The FTIR spectra of graphite (Fig. 4a) indicate the chemical inertness of bulk graphite.[24] Whereas, the FTIR spectra of GEG showed various functional groups (Fig. 4b). A highly intense band at 3428 cm^{-1} was due to the O–H stretching vibration which indicated the presence of OH and/or COOH functional groups within the structure. Very weak bands at 2857 cm^{-1} and 2924 cm^{-1} were due to the symmetric and asymmetric stretching vibration of C–H bond, respectively. Carbonyl C=O stretching vibration (1739 cm^{-1}), C=C stretching vibration of the unoxidized graphitic domain (1641 cm^{-1}), O–H deformation (1462 cm^{-1}), C–O stretching of epoxy groups (1237 cm^{-1}) were seen in the FTIR spectra of GEG.[25,26] Thus, the results obtained from FTIR confirmed the presence of various oxygen containing functional groups such as hydroxyl, epoxy, carboxyl, carbonyl, within the GEG structure. The results of the FTIR analyses performed by Song *et al.*,[27] Marcano *et al.*,[15] Galpaya *et al.*,[24] Bao *et al.*,[28] and Chowdhury *et al.*,[29] were in agreement with the results obtained in the current research.

Scanning electron microscopy (SEM)

Fig. 5 shows the SEM micrographs of both of graphite and GEG. The GEG represented have a lamellar structure with two characteristics figures, (i) aggregated layers in a cluster form, and (ii) needle-like growth. These two different shapes indicate that the microbial isolate has significantly effects on the graphite powder morphology and structure, and a new morphological structure was formed. These results were matched with the Raman and FTIR results which proved the structural change between the original graphite powder and the newly formed GEG structure.

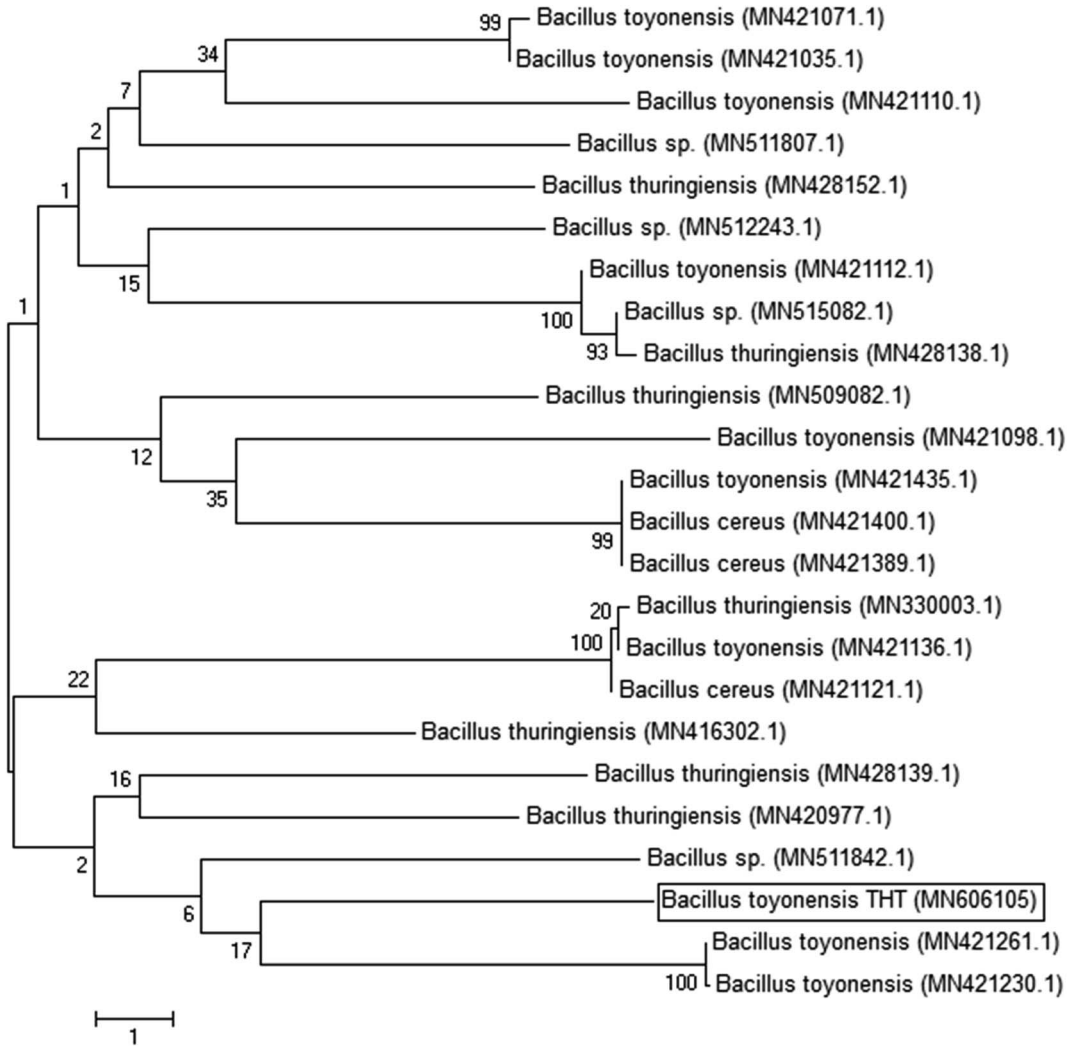

Fig. 6 Phylogenetic position of *Bacillus toyonensis* THT within other related strains deposited in the GenBank. The branching pattern was generated by a neighbor-joining tree method with a bootstrap of 500 and the Genbank accession numbers of the 16S rRNA nucleotide sequences are indicated in brackets.

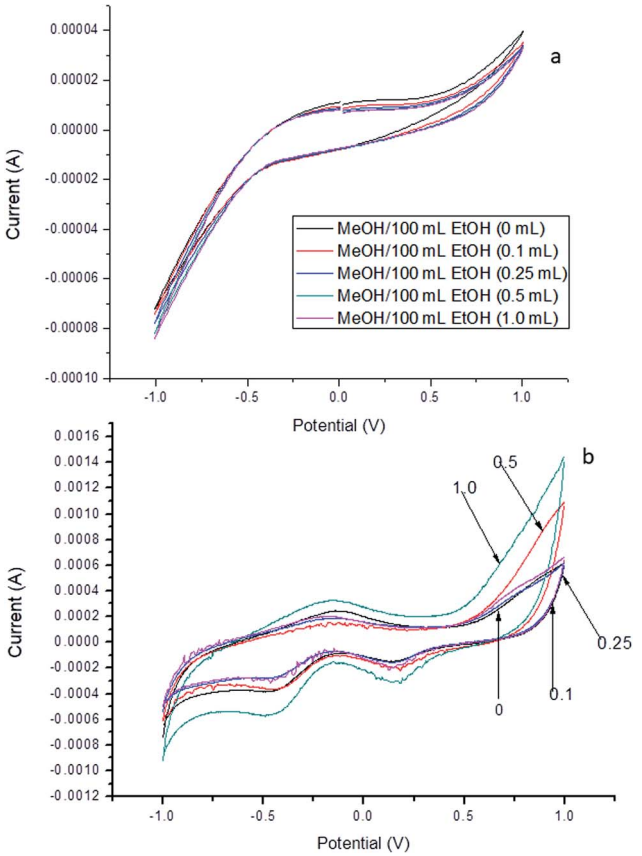

Fig. 7 Cyclic voltammograms of prepared electrodes of (a) G0, and (b) GEG in PBS buffer solution (pH 7.0) with different concentrations of methanol (0–1.0 mL/100 mL buffer).

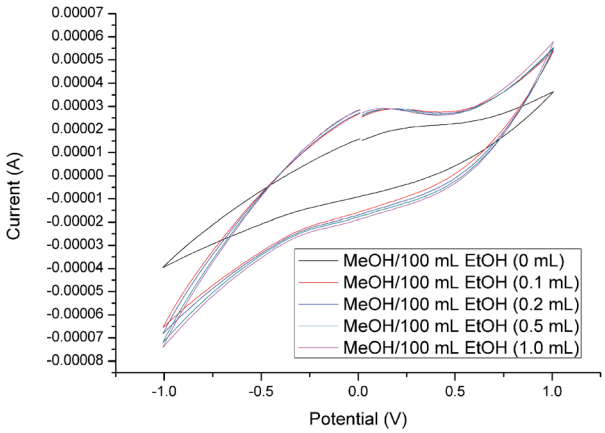

Fig. 9 Cyclic voltammograms of the prepared electrode of GEG in ethanol with different concentrations of methanol (0–1.0 mL/100 mL ethanol).

Suggested BIO mechanism for the formation of GEG structure

The exfoliation of graphite into graphitic layers is practically associated by two primary methods that were applied separately. The first method was mainly dependent on an oxidation process that involves the chemical incorporation of an atom between the sheet flakes of graphite. Liu *et al.*, proposed that the bacterial cells probably produced metabolites that served as surfactants and promoted the contact of the bacterial cells to the graphitic material.[11] This contact can result in extracellular electron transfer pathways at the cell/graphitic material interface that finally resulted in the formation of graphite oxide or graphene oxide.[30] The other method was dependent on an incorporation of a big molecule (other than oxygen) that helped in the exfoliation of the stacked sheets of graphite, which was accompanied by chemical modifications. The current exfoliation mechanism is assumingly attributed to the first method. The large number of oxygen atoms detected by the characterization process outbalanced the ability of the isolated microbe to oxidize the graphite waste and exfoliate its flakes into other oxygenic graphitic structures.

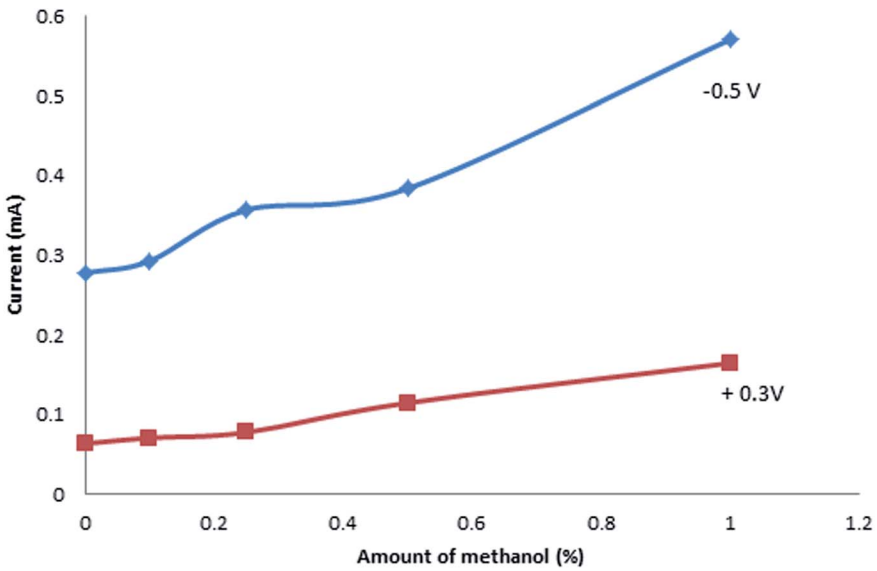

Fig. 8 Calibration curves obtained for methanol at −0.5 V and +0.3 V.

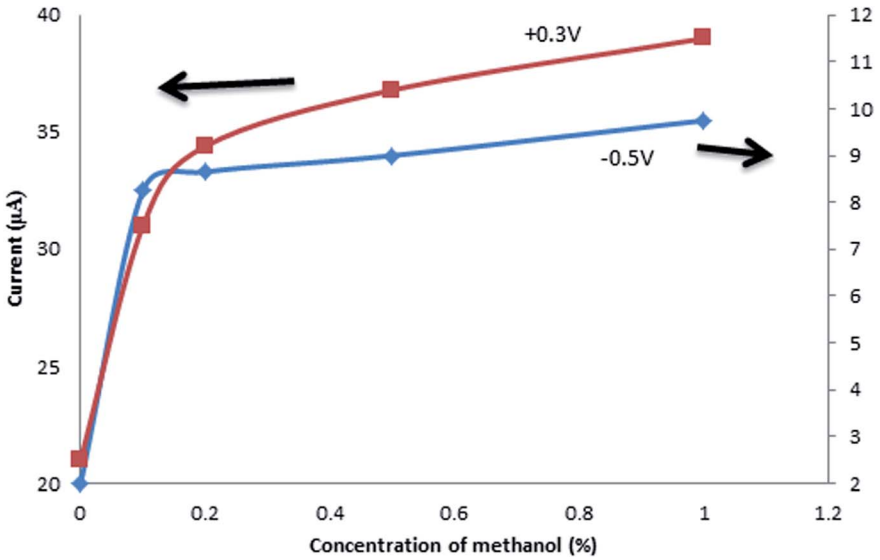

Fig. 10 Calibration curves obtained for methanol in ethanol at −0.5 V and +0.3 V.

Molecular identification of the G3 isolate

The PCR amplification of 16S rRNA from the extracted genomic DNA of isolate G3 showed a 1500 bp amplified band when compared with a 1 kb DNA ladder. The amplified gene obtained was collected from the agarose gel, extracted, purified and submitted to sequencing (Sigma, Germany). The sequence obtained was compared with the 16S rRNA sequences deposited in the GenBank database and revealed that the sequence was 100% similar to that of *Bacillus toyonensis* strains. The sequence was deposited in the GenBank database under the accession number MN606105. The relatedness of the current isolate and other similar strains are represented in the phylogenetic tree shown in Fig. 6.

Electrochemical measurements

In PBS buffer (pH 7.0). Fig. 7 shows the cyclic voltammogram of the prepared electrodes. The biosensor response was tested in 100 mL PBS solution (pH 7.0) in the presence of different amounts of methanol (0.0–0.01 volume ratios). It was noticeable that there were two response ranges at (+0.3 V) and (−0.5 V) for the GEG electrode sample (Fig. 7b). Calibration curves of these two ranges are presented in Fig. 8. The material obtained has remarkable electrochemical sensing to methanol, starting at very low concentrations.

However, the blank graphite electrode (G0) had no sensing behavior towards methanol in PBS buffer solution as shown in Fig. 7a.

The previously described measurements suggest that the sensing mechanism was as follows: firstly, methanol was adsorbed on the electrode surface, which was followed by its dissociation through various steps.[31] The organic intermediate species of methanol oxidation were dissociated on the electrode surface by interacting with the surface OH^- species.[32] Finally, the adsorbed species effected the electrochemical behavior of the electrode.

In ethanol. The same three electrochemical configuration cells were used to distinguish the presence of small amounts of methanol in 100 mL of ethanol.

As shown in Fig. 9, the biosensor response of the GEG electrode towards methanol was tested in 100 mL ethanol in the presence of different concentrations of methanol (0.0–0.01 volume ratios). It was noticeable that, there was a detectable response behavior of the GEG electrode even at relatively low concentrations of methanol. Calibration curves of the two ranges of potential (+0.3 and −0.5 V) are presented in Fig. 10.

The sensing efficiency of the GEG electrode towards methanol in PBS buffer was higher than the detected efficiency in ethanol solution as shown in Fig. 8 and 10. The two regions of potential (+0.3 and −0.5 V) were used in both electrochemical tests of buffer and ethanol media for comparison.

Conclusions

The current work describes the use of green method to substitute the hazardous chemical materials previously used for graphite exfoliation process. The formation of GEG was characterized using Raman and FTIR spectroscopy combined with SEM. The GEG obtained presented high sensitivity toward low concentrations of methanol in both of phosphate buffered saline solution and ethanol. This applied green method is considered to be ecofriendly and a cost-effective method for the bioremediation of graphite waste into valuable graphitic material. It is recommended that more effort is made with this research for the complete exfoliation of graphite into carbon nanostructures.

Conflicts of interest

There are no conflicts to declare.

Acknowledgements

The authors would like to express their gratitude to the Research Center of Advanced Materials – King Khalid University, Saudi Arabia for support with grant number: RCAMS/KKU/002-19.

References

1 G. Maduraiveeran and W. Jin, Nanomaterials based electrochemical sensor and biosensor platforms for environmental applications, *Trends Environ. Anal. Chem.*, 2017, **13**, 10–23.
2 R. Batool, A. Rhouati, M. H. Nawaz, A. Hayat and J. L. Marty, A Review of the Construction of Nano-Hybrids for Electrochemical Biosensing of Glucose, *Biosensors*, 2019, **9**, 46.
3 R. Kumar, B. R. Mehta, M. Bhatnagar, S. Ravi, S. Mahapatra, S. Salkalachen and P. Jhawar, Graphene as a transparent conducting and surface field layer in planar Si solar cells, *Nanoscale Res. Lett.*, 2014, **9**, 349.
4 A. A. Balandin, S. Ghosh, W. Bao, I. Calizo, D. Teweldebrhan, F. Miao and C. N. Lau, Superior thermal conductivity of single-layer graphene, *Nano Lett.*, 2008, **8**, 902–907.
5 B. Marinho, M. Ghislandi, E. Tkalya, C. E. Koning and G. de With, Electrical conductivity of compacts of graphene, multi-wall carbon nanotubes, carbon black, and graphite powder, *Powder Technol.*, 2012, **221**, 351–358.
6 X. Zhu, J. Li, H. He, M. Huang, X. Zhang and S. Wang, Application of nanomaterials in the bioanalytical detection of disease-related genes, *Biosens. Bioelectron.*, 2015, **74**, 113–133.
7 S. Shi, W. Jiang, T. Zhao, K. E. Aifantis, H. Wang, L. Lin, Y. Fan, Q. Feng, F. z. Cui and X. Li, The application of nanomaterials in controlled drug delivery for bone regeneration, *J. Biomed. Mater. Res., Part A*, 2015, **103**, 3978–3992.
8 V. Palermo, I. A. Kinloch, S. Ligi and N. M. Pugno, Nanoscale mechanics of graphene and graphene oxide in composites: a scientific and technological perspective, *Adv. Mater.*, 2016, **28**, 6232–6238.
9 Y. Liu, H. Cai, F. Wang, J. Wang, Q. Huang, Z. Fu and Y. Lu, Graphene on {116} faceted monocrystalline anatase nanosheet array for ultraviolet detection, *Nanoscale*, 2018, **10**, 3606–3612.
10 B. A. Lehner, V. A. Janssen, E. M. Spiesz, D. Benz, S. J. Brouns, A. S. Meyer and H. S. van der Zant, Creation of Conductive Graphene Materials by Bacterial Reduction Using *Shewanella oneidensis*, *ChemistryOpen*, 2019, **8**, 888–895.
11 L. Liu, C. Zhu, M. Fan, C. Chen, Y. Huang, Q. Hao, J. Yang, H. Wang and D. Sun, Oxidation and degradation of graphitic materials by naphthalene-degrading bacteria, *Nanoscale*, 2015, **7**, 13619–13628.
12 B. Chen, H. Huang, X. Ma, L. Huang, Z. Zhang and L.-M. Peng, How good can CVD-grown monolayer graphene be?, *Nanoscale*, 2014, **6**, 15255–15261.
13 Y. Zhang, L. Zhang and C. Zhou, Review of chemical vapor deposition of graphene and related applications, *Acc. Chem. Res.*, 2013, **46**, 2329–2339.
14 S. Abdolhosseinzadeh, H. Asgharzadeh and H. S. Kim, Fast and fully-scalable synthesis of reduced graphene oxide, *Sci. Rep.*, 2015, **5**, 10160.
15 D. C. Marcano, D. V. Kosynkin, J. M. Berlin, A. Sinitskii, Z. Sun, A. Slesarev, L. B. Alemany, W. Lu and J. M. Tour, Improved synthesis of graphene oxide, *ACS Nano*, 2010, **4**, 4806–4814.
16 C. K. Chua and M. Pumera, Chemical reduction of graphene oxide: a synthetic chemistry viewpoint, *Chem. Soc. Rev.*, 2014, **43**, 291–312.
17 H. C. Schniepp, J.-L. Li, M. J. McAllister, H. Sai, M. Herrera-Alonso, D. H. Adamson, R. K. Prud'homme, R. Car, D. A. Saville and I. A. Aksay, Functionalized single graphene sheets derived from splitting graphite oxide, *J. Phys. Chem. B*, 2006, **110**, 8535–8539.
18 R. Paasma, K. E. Hovda and D. Jacobsen, Methanol poisoning and long term sequelae–a six years follow-up after a large methanol outbreak, *BMC Clin. Pharmacol.*, 2009, **9**, 5.
19 X.-Y. Zou, R. Xie, X.-J. Ju, W. Wang, Z. Liu, X.-Y. Li and L.-Y. Chu, Visual detection of methanol in alcoholic beverages using alcohol-responsive poly(*N*-isopropylacrylamide-*co*-*N*,*N*-dimethylacrylamide) copolymers as indicators, *RSC Adv.*, 2014, **4**, 61711–61721.
20 A.-S. Al-Sherbini, M. Bakr, I. Ghoneim and M. Saad, Exfoliation of graphene sheets *via* high energy wet milling of graphite in 2-ethylhexanol and kerosene, *J. Adv. Res.*, 2017, **8**, 209–215.
21 A. C. Ferrari, Raman spectroscopy of graphene and graphite: disorder, electron–phonon coupling, doping and nonadiabatic effects, *Solid State Commun.*, 2007, **143**, 47–57.
22 C. Wongchoosuk and Y. Seekaew, *2D Materials*, 2019.
23 S. Roscher, R. Hoffmann and O. Ambacher, Determination of the graphene–graphite ratio of graphene powder by Raman 2D band symmetry analysis, *Anal. Methods*, 2019, **11**, 1224–1228.
24 D. Galpaya, M. Wang, G. George, N. Motta, E. Waclawik and C. Yan, Preparation of graphene oxide/epoxy nanocomposites with significantly improved mechanical properties, *J. Appl. Phys.*, 2014, **116**, 053518.
25 N. A. Kumar, S. Gambarelli, F. Duclairoir, G. Bidan and L. Dubois, Synthesis of high quality reduced graphene oxide nanosheets free of paramagnetic metallic impurities, *J. Mater. Chem. A*, 2013, **1**, 2789–2794.
26 Y. Huang, M. Zeng, J. Ren, J. Wang, L. Fan and Q. Xu, Preparation and swelling properties of graphene oxide/poly (acrylic acid-*co*-acrylamide) super-absorbent hydrogel nanocomposites, *Colloids Surf., A*, 2012, **401**, 97–106.
27 J. Song, X. Wang and C.-T. Chang, Preparation and characterization of graphene oxide, *J. Nanomater.*, 2014, **2014**, 276143.
28 C. Bao, L. Song, W. Xing, B. Yuan, C. A. Wilkie, J. Huang, Y. Guo and Y. Hu, Preparation of graphene by pressurized oxidation and multiplex reduction and its polymer

nanocomposites by masterbatch-based melt blending, *J. Mater. Chem.*, 2012, **22**, 6088–6096.

29 D. R. Chowdhury, C. Singh and A. Paul, Role of graphite precursor and sodium nitrate in graphite oxide synthesis, *RSC Adv.*, 2014, **4**, 15138–15145.

30 G. Wang, F. Qian, C. W. Saltikov, Y. Jiao and Y. Li, Microbial reduction of graphene oxide by *Shewanella*, *Nano Res.*, 2011, **4**, 563–570.

31 D.-S. Park, M.-S. Won, R. N. Goyal and Y.-B. Shim, The electrochemical sensor for methanol detection using silicon epoxy coated platinum nanoparticles, *Sens. Actuators, B*, 2012, **174**, 45–50.

32 B. Tao, J. Zhang, S. Hui, X. Chen and L. Wan, An electrochemical methanol sensor based on a Pd–Ni/SiNWs catalytic electrode, *Electrochim. Acta*, 2010, **55**, 5019–5023.